RSC Advances

ROYAL SOCIETY OF CHEMISTRY

www.rsc.org/advances

A Novel Cementitious Microfiltration Membrane: Mechanisms of Pore Formation and Properties for Water Permeation

Zhe Wang, Zhonglin Chen, Jing Chang, Jimin Shen, Jing Kang, Lei Yang, Qian Chen*

(State Key Laboratory of Urban Water Resource and Environment, School of Municipal & Environmental Engineering, Harbin Institute of Technology, Harbin 150090, China)

Corresponding author e-mail: shenjimin@hit.edu.cn; Tel: +86–451-86287000; fax: +86–451-86283028.

Abstract:

This study involved the fabrication of a novel low-cost microfiltration membrane using quartz and cement. The entire fabrication process was conducted at room temperature, rather than utilizing high-temperature sintering, as is generally used during the fabrication of traditional inorganic membrane. The mean pore size of the membrane ranged from 0.4 to 2.4 μm depending on the quartz-to-cement ratio (q/c) used. Two types of pores (I and II) were formed in the membrane. The formation of type I pores was mainly attributed to the stacking of cement particles. The formation of type II pores, which were less prevalent than type I pores, was attributed to the division of bigger pores by the thin needle-like ettringite. The sizes of the type I and type II pores varied significantly, depending on the used q/c. Moreover, investigation of the membrane properties showed that as the q/c used increased, increases were obtained for both the membrane porosity (from 18.4% to 31.4%) and water flux (from 0.16 to 13.26 $m^3 \cdot m^{-2} \cdot h^{-1} \cdot bar^{-1}$), whereas the bending strength decreased (from 9.75 to 3.54 MPa). Additionally, element dissolution experiments demonstrated that the membrane was suitable for use for water treatment.

Introduction

The World Health Organization estimates that 1 billion people currently do not have access to clean, piped water.[1] The challenge of providing acceptable drinking water is further expanded by population growth, industrialization, the contamination of available freshwater resources and climate change.[2] In developing countries, this situation is severe, and the development of a cheap and efficient water treatment process is particularly valuable.

In the water treatment process, microfiltration has been used broadly because of its low cost, high flux and simpler production procedures.[3-6] According to the membrane materials used, microfiltration membranes can be divided into two categories: organic and inorganic membranes. Compared to organic membranes, inorganic membranes have many advantages, such as chemical stability (e.g., ozone resistance), pressure resistance, insensitivity to bacterial action, the steam sterilizability and a longer lifetime.[7, 8] Therefore, inorganic membranes have gradually attracted the attention of researchers and have been applied to purify contaminated water.[9-11] Furthermore, the inorganic microfiltration membrane can be used as a pretreatment in the water desalination process, and it can also be used as a support membrane for the fabrication of inorganic ultrafiltration and nanofiltration membrane. However, the current commercial inorganic membranes are not suitable for large-scale water treatment processes because of their high cost, which is a result of the use of expensive raw materials (e.g., alumina, zirconia and titania) and the high sintering temperature required.[12] To address this issue, some low-cost raw materials, such as kaolin[13-15], fly ash[16], clay[17-19], mullite[20, 21] and natural zeolite[22], have been progressively used to fabricate inorganic membranes. However, the development of technologies to avoid the sintering process during inorganic membrane production has received little attention in recent studies.

Portland cement is commonly used in building and is characterized by good strength. Cement contains many impure chemical constituents, most of which are tricalcium (C3S), dicalcium silicate (β-C2S), tricalcium aluminate (C3A) and alumino-ferrite phases (C4AF).[23, 24] These compounds can react with water under ambient conditions and produce relatively insoluble hydration products. Based

on the above, the fabrication of a new type of inorganic membrane under ambient conditions using low-cost cement is valuable. However, hydrated cement has worse water permeability than traditional inorganic microfiltration membrane due to the limited porosity and small pore size.[25] To solve the problem, many cement-based materials have been used to permeate water in the engineering applications. For example, larger aggregates were mixed with smaller cement particles to produce a pervious pavement, which was used to transport large volumes of water through the material structure to eliminate the problems of storm-water runoff and rainwater acidification.[26-28] Therefore, in this study, the uniformly larger quartz particles were added to the system of cement and water. The quartz particles could disrupt the growth of the cement hydration products and thereby increase the porosity and pore size of this novel cementitious membrane.

In this study, we reported a novel low-cost microfiltration membrane that was fabricated with cement and quartz at room temperature. The membranes were fabricated with various quartz-to-cement ratios (q/c), and the resulting microstructures were investigated to explain the mechanisms of the formation of membrane pores. Furthermore, the permeability, bending strength and element stability of the membrane were also investigated to verify its potential for various applications.

Experimental

Raw materials

Quartz (≥ 99.0%, Xi Long Chemical Co., Ltd., China) and Portland cement (PO 42.5, Tian E®, China) were used as the raw materials for the fabrication of the cementitious microfiltration membrane. Chemical composition of the Portland cement used in this research was listed in the Supplementary Material (Table S1) to facilitate the reproducibility of this membrane.

Membrane fabrication

The membranes were produced using quartz, cement and deionized water. The quartz-to-cement weight ratios (q/c) used ranged from 0.3 to 4.0, as shown in Table 1. Fabrication of the cementitious

membrane was based on a dry press molding process. First, the quartz particles were added to the cement particles, followed by dry-mixing for 2 min (10 r/s) in a stainless-steel agitator. An appropriate amount of deionized water was then introduced into the mixture with stronger mechanical stirring (30 r/s) to prepare a paste. Next, 10.5 g of the paste was placed into a circular stainless-steel mold consisting of a ring (70-mm outer diameter, 50-mm inner diameter and 3-mm thickness) and a desk (70-mm diameter and 3-mm thickness). A thin plastic sheet was sandwiched between the ring and the desk to facilitate separation of the paste from the mold. The mold was then carefully transported to a pressure shaping machine, and the paste was pressed at 6 MP for 1 min. Next, the mold was placed in a standard curing box (Shang Hai Jing Hong Laboratory Instrument Co., Ltd., China), in which the temperature and humidity were controlled at 20 °C and 95%, respectively. After 48 h, the shaped paste was taken out of the mold and stored in the standard curing box again for 10 days. Ten days later, the cementitious microfiltration membrane was formed, with a diameter of 50 mm and a thickness of 3 mm. Finally, the membrane was polished by abrasive paper to ensure that it was smooth and flat.

Characterization methods

The phase composition of the raw materials was identified by X-ray diffraction (XRD), which was carried out on a Rigaku D/max-rA diffractometer with Cu K_α radiation (λ= 1.5405 Å). The particle size distributions of the raw materials were measured by dynamic light scattering using a Mastersizer 2000 apparatus (Malvern Instrument Co., Ltd., UK).

The surface and cross-section morphologies of the membranes were characterized by scanning electron microscopy (SEM, Quanta 200FEG, FEI Corp., USA) to observe the connection between the quartz and cement particles.

The pore size and distribution of the membranes were measured using a pore size distribution analyzer (PSDA) (Nan Jing Gao Qian Functional Materials Co., Ltd., China) according to the gas-liquid displacement method[29]. The PSDA could measure the diameters of the opened pores in the membrane in the range of 0.1 to100 μm using a precise mass flow meter and a gaseous pressure sensor.

The accuracy and stability of the PSDA was verified by measuring three membranes that were produced under the same condition. The results were listed in Fig. S1.

The porosity of the membrane was measured according to the Archimedes method[30] using water as the immersing medium, as specified in ASTM C20-00. All the porosities measured in this study were the open porosity of the membrane.

The elemental composition of the membrane was tested using an X-ray fluorescence spectrometer (XRF, AXIOS-PW 4400, PANalytical, Netherlands).

The water permeation experiments were carried out using a laboratory-made setup (Fig. 1). The setup consisted of a cylindrical container (stainless steel) for storing water, a base (stainless steel) for loading the membrane and a Teflon packing plate for sealing. The entire setup was fastened to the sample using a stainless-steel clip. A nitrogen cylinder was connected to the inlet of the cylindrical container to pressurize the water (deionized water, 25 ^{o}C). The water permeation tests involved the measurement of the permeated liquid volume within 10 min under various trans-membrane pressure drops (40–160 kPa) that were typically used in microfiltration. The practical permeation area of the membrane was 7 cm^2. The experiments were repeated three times.

The bending strength of the membrane was tested by the three point bending method[15] using a universal testing machine (Instron 5569, Instron Corporation, U.S.), with a span length of 30 mm. The samples were 3 mm × 4 mm × 40 mm rectangular bars.

An atomic emission spectrometer (ICP-AES, Optima 5300DV, Perkin Elmer, U.S.) was used to detect the elements in the membrane effluent to access the safety of the membrane materials.

Results and Discussion

Characterization of the raw materials

The XRD spectra of cement and quartz particles are presented in Fig. 2a-b. Fig. 2a shows that the cement contains multiple man-made chemical constituents, including Ca_3SiO_5, Ca_2SiO_4, $Ca_3Al_2O_6$,

Ca_2AlFeO_5 and SiO_2, as the main composition of the ordinary Portland cement.[24] The XRD spectrum of the quartz (Fig. 2b) is in agreement with the JCPDS database file (PDF# 99-0088) which indicates that the quartz used in the work is ideal quartz (SiO_2). The particle size distributions of the quartz and cement are shown in Fig. 2c. Quartz particles in the range of 28.6 to 81.5 μm (D_{50}=50.0 μm) and cement particles in the range of 3.0 to 33.4 μm (D_{50}=14.6 μm) are obtained by screening. In the membrane, the quartz can act as a support and the cement can act as a binder, filling in the gaps between the quartz particles. Deionized water is used to induce the hydration reaction of the cement.

Microstructure observation and pore characterization of the membrane

The microstructures of the membranes are investigated to observe the stacking of raw particles in the membrane. The results in Fig. 3a-e show the surface morphology of the novel membranes at different weight ratios of quartz-to-cement (q/c). In the membrane structures, the supporting function of the quartz particles gradually increases as the used q/c increased, and the smaller cement particles are embedded on the surface of the quartz particles and facilitate binding. Furthermore, Fig. 3 shows that a similar stacking structure of particles is observed for the cementitious membrane and the conventional sintered membrane (a Al_2O_3/TiO_2 membrane)[31]. This may be because the larger-sized quartz and Al_2O_3 particles play a similar supporting function and the smaller-sized cement and TiO_2 particles act as the source of binding phase in the respective membranes. In the traditional sintered Al_2O_3/TiO_2 membrane, TiO_2 with smaller size order is normally used as a sintering promoter agent for the reason that titania can react with alumina to form aluminum titanate (Al_2TiO_5) through solid-state reactions (above 1280 ^oC) at necks between the larger-sized alumina particles.[31] Therefore, in this sintered membrane, the pores form from the stacking of alumina particles by the newly formed Al_2TiO_5 phase. Analogously, in the novel cementitious membrane, the larger-sized quartz can be recommended as the membrane support which partly replaces the above function of alumina (besides being a support, the alumina also participates in the solid-state reaction), and the smaller sized cement plays a binding function, similar to the aforementioned Al_2TiO_5 phase. However, the cementitious membrane can be fabricated under

ambient conditions, unlike the sintered Al_2O_3/TiO_2 membrane.

The pore size distributions of the membranes are studied, as shown in Fig. 4. The results indicate that the membrane pores are mainly single micrometers in size (< 8 μm) with a narrow size distribution, which results from the narrow particle size distribution of the raw materials. Moreover, with the increase in the q/c used in the membrane, the pore size distribution changes significantly from a unimodal distribution to a bimodal distribution. It is possible that a new type of pores forms in the membrane at higher q/c. The results in Fig. 5 show that the mean pore size of the membranes increases significantly from 0.4 μm to 2.4 μm as the q/c increases from 0.3 to 4.0. Over the same q/c range, the membrane porosity also increases from 18.4% to 31.4%. Therefore, increasing the percentage of quartz in the raw materials can significantly improve the pore size and porosity of the novel membrane.

Pore formation mechanisms of the membrane

The gas-liquid displacement method and SEM can measure the pore size of inorganic microfiltration membranes. Therefore, the results of these two methods shall be authenticated reciprocally. For example, in the traditional Al_2O_3/TiO_2 membrane[31], the pore size measured by the gas-liquid displacement method is 6.8 μm, similar to the pore size shown in its SEM image. Because the cementitious membrane has a similar particle stacking structure compared with the traditional sintered membrane, which is mentioned above. Therefore, the particle stacking mold is also the most likely mechanism of the pore formation for the cementitious membrane. However, the pore size of the cementitious membrane detected by the SEM images (Fig. 3b-e, pore size > 10.0 μm) differs significantly from that detected by the pore size analyzer (Fig. 4c-f, 1.0-2.5 μm), especially when using a high q/c to fabricate the membrane. The differences in the pore sizes detected by the SEM images and the pore size analyzer indicate that the pore formation mechanisms of the cementitious membrane may have a certain particularity compared with the traditional membrane. The macro-pores from the larger-sized quartz stacking (shown in Fig. 3) are not the primary pores of the cementitious membrane.

To investigate the pore formation mechanisms of the novel membrane, the relationship between

the pore size of the membrane and the particle size of the raw materials is studied based on the supposition that the pores of the novel membrane are also formed from the stacking of particles. Some researchers previously reported the following relationship between the pore diameter and the particle diameter:

$$\frac{d_{mod}}{P_{50}} = -0.515\ln(1-\varepsilon) \quad (1)$$

In equation 1, "d_{mod}" is the modal equivalent pore diameter, "P_{50}" is the mean particle diameter and "ε" is the porosity of the membrane.[32] When applied to the cementitious membrane studied here, using the average value of ε in Fig. 5 (25.3%), equation 1 can be rewritten as follows:

$$d_{mean} = 0.150\ D_{mean} \quad (2)$$

In which "d_{mean}" and "D_{mean}" represent the mean diameters of the accumulated pores and the raw material particles, respectively.

Fig. 2c shows that the D_{mean} of the cement particles is 14.6 μm and the D_{mean} of the quartz particles is 50.0 μm. Inserting the D_{mean} of the cement into equation 2, the d_{mean} of the cement is 2.2 μm, which represents the size of pores resulting from the cement particle stacking. This result is close to the membrane pore size, especially for the membrane produced at high q/c (Fig. 4e-f). Moreover, this value is only based on a cement particle stacking mode. At a low q/c (a relative large amount of cement), more cement hydration products will form and fill the cement stacking pores to decrease the membrane pore size. Therefore, if the growth of the cement hydration products on the surface of the cement particles is considered, the pore size shall be smaller, which produces a value closer to the mean pore size of the membrane fabricated at low q/c (Fig. 4a-b, only about 0.5 μm). In the same way, inserting the D_{mean} of the quartz into equation 3, the d_{mean} of the quartz is 7.5 μm, which represents the size of pores resulting from quartz particle stacking. This result is consistent with the largest-sized pores (6.5-8.0 μm) in every pore size distribution curve in Fig. 4. However, these macro-pores only

occupy a small proportion of the total pores. Based on the above findings, it is possible that most of the opened pores in the cementitious membrane result from the stacking of the cement particles. The growth of the cement hydration products can decrease the size of pores, and this function is more obviously when increasing the amount of cement used.

To confirm the above pore-formation supposition, the connection part between the cement particles in the membrane are observed by SEM (using a high magnification of 20000), and a convincing result is obtained (Fig. 6a-c). The SEM images reveal that the pores form in the connections of the cement particles. The pore sizes in Fig. 6b and c are close to the results in Fig. 4d and f, respectively. Therefore, the formation of most pores in the cementitious membrane results from the stacking and connection of the cement particles. Moreover, at low q/c (Fig. 6a), the cement hydration products grow densely and the membrane pores are closed. As q/c increases from 0.5 to 4.0, the cement hydration products become sparse, and the membrane pores gradually open (Fig. 6a-c). This result can be explained from two perspectives. On one hand, when the membrane is produced with a high q/c, such as in Fig. 6c, the water-to-cement ratio of the membrane is also high, as shown in Table 1. Under this condition, water can occupy much more space in the membrane in the initial membrane production process. During the cement hydration reaction, the water is gradually consumed. Therefore, the greater amount of space occupied by the water is gradually vacated, and a higher membrane porosity can be obtained. On the other hand, the contact area between the cement particles is lower when a high q/c is used; thus, the growth of the cement hydration products is unfavorable. Therefore, at high q/c, the pore size of membrane (1-2 μm, Fig. 4f and Fig. 6c) is closer to the result for the cement particle stacking mode (2.2 μm, as mentioned above), and the membrane pores are insufficiently filled by the hydrated products of cement. In contrast, in the membrane produced at low q/c (Fig. 6a), there is less space among cement particles, leading the cement hydration products to grow densely and fill much more space among the cement particles. Therefore, the membrane pores are filled sufficiently by the hydrated products in this type of membrane, and the membrane pore size

(< 0.5 μm, Fig. 4a) is significantly affected.

Fig. 6d-f show that higher q/c values corresponds to the growth of more needle-like compounds in the membrane pores. At high q/c, these needles grow longer and cross one another, dividing the membrane pores (Fig. 6f), which may increase the proportion of smaller pores in the membrane. This explanation is supported by the PSDA results in Fig. 4, which indicate that with increasing q/c, a new peak appears and increases in intensity. This new peak corresponds to a smaller pore size than the prominent peak in the pore size distribution curve does. These newly formed pores may result from the needle-like compounds dividing the larger membrane pores. Moreover, as the q/c increases, these needle-like compounds become more expansive, and their dividing function is more prominent (Fig. 6f). To clarify the source and composition of these needle-like compounds, EDX analysis is carried out, and the results are shown in Fig. 7c-d. The testing area of the EDX analysis is marked with a red box in the corresponding SEM images (Fig. 7a: the needle-like structure; Fig. 7b: the adjacent flat area). The result shows that in the needle-like compound structure, the contents of Al, S and Fe increase by 2.15, 1.10 and 4.42 times, respectively, compared to the adjacent flat area. The elements Al and S are characteristic of the ettringite, which results from the reaction of the calcium aluminate and the artificially added calcium sulfate. The element Fe is also involved in the formation of ettringite.[23, 33-37] Moreover, the ettringite has been found to have a needle-like structure in many studies.[23, 34, 38] Thus, it is believed that the needle-like structure observed in this study is ettringite.

Based on the above analysis, details about the reactive process for the membrane formation are summarized as: (1) dry mixing of materials; (2) wet mixing of materials; (3) shaping by dry pressing; (4) membrane curing. In the first step, the dry mixing of quartz and cement particles results in that the larger-sized quartz particles are surrounded by the smaller-sized cement particles. Then in the second step of wet mixing, water is added and occupies the space among the particles. The third step of dry pressing decreases the pore volume of the system, resulting in that the distances between quartz particles are closer. Therefore, the cement particles are much closer with each other. In the fourth step

of membrane curing, cement hydration reaction occurs, and the cement particles react with water to form multiple membrane binding phases ($Ca_3SiO_5 \cdot nH_2O$, $Ca_2SiO_4 \cdot nH_2O$, $Ca_3Al_2O_6 \cdot nH_2O$ and $Ca_2AlFeO_5 \cdot nH_2O$, etc). This reaction gradually consumes the water. Great amount of spaces occupied by the water is gradually vacated in this stage, which supplies spaces for the further growth of these binding phases. These binding phases have 2 vital functions. On one hand, they connect the cement particles together, which fixing the quartz particles in the membrane, and increasing the strength of the membrane. On the other hand, the cement particles, which stack among the quartz particles, are connected by these binding phases to form the membrane pores. Moreover, with increasing q/c in the membrane fabrication process, ettringite can significantly widen the pore size distribution of the membrane, as observed in Fig. 4.

Water permeation test

The membrane water flux J ($m^3 \cdot m^{-2} \cdot s^{-1}$) is affected by many factors and can be estimated according to the Hagen–Poiseuille equation[39] :

$$J = \frac{n\pi r^4 \Delta P}{8\mu l} = L_h \Delta P \quad (3)$$

In which the L_h ($m^3 \cdot m^{-2} \cdot s^{-1} \cdot Pa^{-1}$) is the hydraulic permeability of the membrane, ΔP (Pa) is the trans-membrane pressure drop, μ is the water viscosity, l is the pore length and r is the mean pore radius of the membrane. Using ε ($=n\pi r^2$) to represent the membrane porosity, the water permeability of the membrane (L_h) can be expressed by the following equation, which is derived from Eq. 3:

$$L_h = \frac{\varepsilon d^2}{32\mu l} \quad (4)$$

In which d is the mean pore size of the membrane.

The novel microfiltration membranes that are fabricated at different q/c are subjected to the water permeation test using deionized water. Fig. 8 shows the changes in the water fluxes (J) of the membrane under a varying trans-membrane pressure drop (40-160 kPa). The slopes of these flux

curves can represent the water permeability (L_h) of the membrane used. As shown in Fig. 8, the water flux of each membrane has an excellent linear relationship with the trans-membrane pressure drop, which is consistent with equation 3. Moreover, the water permeability of the membrane increases markedly from 0.16 to 13.26 $m^3 \cdot m^{-2} \cdot h^{-1} \cdot bar^{-1}$ when the used q/c increases from 0.3 to 4.0. These results can be explained by the increase of the porosity and the mean pore size of the membrane, as shown in Fig. 5. Furthermore, according to equation 4, the water permeability is directly proportional to the mean pore size and the porosity of the membrane. Therefore, the water fluxes of the membranes fabricated at the high q/c (Fig. 8d-f) increase more obviously than that of the membranes fabricated at the low q/c (Fig. 8a-c) when the trans-membrane pressure drop increases. Compared to some traditional inorganic microfiltration membranes[15, 40], the cementitious microfiltration membranes fabricated at high q/c in this study (Fig. 8d-f) have a comparable water permeability, based on similar porosities and pore sizes. However, the porosity of the cementitious membrane is approximately 30%, which limits the increase of the membrane permeation flux, compared to some traditional inorganic membranes with high porosity (e.g., the aforementioned Al_2O_3/TiO_2 membrane with a porosity of 35%-45% and a water permeability of 25-40 $m^3 \cdot m^{-2} \cdot h^{-1} \cdot bar^{-1}$). The low cost of the cementitious membrane can possibly cover this shortage in the water treatment process.

Mechanical strength analysis

The mechanical strength of the prepared membrane is tested using the three-point bending strength method. The bending strength of the membrane, shown in Fig. 9, decreases markedly from 9.75 to 3.54 MPa as the used q/c increases from 0.3 to 4.0. This result can be attributed to the decrease of the cement proportion and the increase of the porosity in the membrane. In this study, the bending strength of the membranes with available water permeability (such as the membranes tested in Fig. 8d-f) can reach approximately 5 MPa. However, this value is still substantially less than that of traditional sintered membranes[15, 41, 42] (5-45 MPa, commonly). The sintered inorganic membrane is mainly designed for use in the field of chemical engineering, in which the membrane often works under high

temperature and high pressure and thus requires the high strength. However, the cementitious membrane is intended for use in the water treatment process; as a result, the limited bending strength of this membrane is considered to be sufficient.

Element dissolution tests

Cement is a multiphase composite material and contains many elements, some of which are heavy metals and are harmful for health when present in the water supply. The potential contamination of heavy metals is becoming a concern.[43-45] X-ray fluorescence (XRF) spectrometry is used to identify the elemental composition of the membrane. The tested membrane is produced using a q/c of 3.0. The result is shown in Table 2, and it indicates that many of the elements existing in the membrane are limited in the national drinking water standard of China (GB5749-2006)[46] and the drinking water standards of the U.S. Environmental Protection Agency (EPA)[47]. Therefore, it is necessary to test the element contents in the membrane effluent to ensure the safety of the cementitious membrane. The experiment is performed using two trans-membrane pressure drops (20 kPa and 60 kPa). The results in Table 2 show that the concentrations of almost all of the element contents in the membrane effluent are lower than the limits set by the two drinking water standards considered for both the high (60 kPa) and low (20 kPa) trans-membrane pressure drops. The concentrations of the element Al obtained from the high and low pressure drop effluents (0.09 and 0.13 mg/L, respectively) exceed the maximum limit set by the EPA (0.05 mg/L) but are lower than the limit set by GB5749-2006 of China (0.2 mg/L). Other harmful metals, such as Cr, Mn, Cu, Zn and Pb are not detected in the effluent samples. The results verify the safety of this novel membrane material.

Conclusions

A novel cementitious microfiltration membrane was prepared for water treatment with different quartz-to-cement ratios (q/c). The mechanisms of membrane pore formation can be summarized as follows. (1) The formation of the largest-sized pores was mainly attributed to the stacking of quartz

particles, and the pore size was 6–8 μm. This pore type was formed under every q/c used in this study, comprising a small proportion of all pores in the sample. (2) The more prevalent pores in the membrane resulted from the stacking of the cement particles. The sizes of these pores ranged from 0.3 to 2.5 μm depending on the used q/c. (3) The aforementioned dominant pores could be divided by thin needle-like ettringites, forming smaller pores. Furthermore, the membrane properties were also studied. With the increasing q/c used in the membrane, the membrane porosity and water flux were improved; however, the bending strength decreased significantly. The element dissolution tests proved that the concentrations of the elements in the membrane effluent were lower than the limits set by China's national drinking water standard. Therefore, the cementitious membrane is a safe material that can be used in the water treatment process.

Acknowledgments

This work was supported by the Fund for Creative Research Groups of China (Grant No. 51121062), the State Key Laboratory of Urban Water Resource and Environment (Harbin Institute of Technology) (No. 2014DX02) and the National Important Items of Science and Technology for the Control and Treatment of Water Pollution (Grant No. 2014ZX07405002).

Reference

1. R. F. Service, *Sci.*, 2006, 313, 1088-1090.
2. M. Elimelech and W. A. Phillip, *Sci.*, 2011, 333, 712-717.
3. I. Jedidi, S. Khemakhem, A. Larbot and R. B. Amar, *Ceram. Int.*, 2009, 35, 2747-2753.
4. G. Belfort, R. H. Davis and A. L. Zydney, *J. Membr. Sci.*, 1994, 96, 1-58.
5. W. Yuan and A. L. Zydney, *J. Membr. Sci.*, 1999, 157, 1-12.
6. Q. B. Chang, J. E. Zhou, Y. Q. Wang, J. Liang, X. Z. Zhang, S. Cerneaux, X. Wang, Z. W. Zhu and Y. C. Dong, *J. Membr. Sci.*, 2014, 456, 128-133.
7. A. Larbot, J. P. Fabre, C. Guizard, L. Cot and J. Gillot, *J. Am. Ceram. Soc.*, 1989, 72, 257-261.
8. B. S. Karnik, S. H. Davies, M. J. Baumann and S. J. Masten, *Environ. Sci. Technol.*, 2005, 39, 7656-7661.

9. N. W. Gao, M. Li, W. H. Jing, Y. Q. Fan and N. P. Xu, *J. Membr. Sci.*, 2011, 375, 276-283.

10. D. Vasanth, G. Pugazhenthi and R. Uppaluri, *J. Membr. Sci.*, 2011, 379, 154-163.

11. B. Zhu, Y. X. Hu, S. Kennedy, N. Milne, G. Morris, W. Q. Jin, S. Gray and M. Duke, *J. Membr. Sci.*, 2011, 378, 61-72.

12. Y. C. Dong, X. Y. Feng, D. H. Dong, S. L. Wang, J. K. Yang, H. F. Gao, X. Q. Liu and G. Y. Meng, *J. Membr. Sci.*, 2007, 304, 65-75.

13. F. Bouzerara, A. Harabi, S. Achour and A. Larbot, *J. Eur. Ceram. Soc.*, 2006, 26, 1663-1671.

14. B. K. Nandi, B. Das, R. Uppaluri and M. K. Purkait, *J. Food Eng.*, 2009, 95, 597-605.

15. J. N. Zhou, X. Z. Zhang, Y. Q. Wang, A. Larbot and X. B. Hu, *J. Porous Mater.*, 2010, 17, 1-9.

16. I. Jedidi, S. Saidi, S. Khmakem, A. Larbot, N. Elloumi-Ammar, A. Fourati, A. Charfi and R. Ben Amar, *Arab. J. Chem.*, 2009, 2, 31-39.

17. N. Saffaj, M. Persin, S. A. Younsi, A. Albizane, M. Cretin and A. Larbot, *Appl. Clay Sci.*, 2006, 31, 110-119.

18. S. Khemakhem, A. Larbot and R. Ben Amar, *Ceram. Int.*, 2009, 35, 55-61.

19. S. Jana, M. K. Purkait and K. Mohanty, *Appl. Clay Sci.*, 2010, 47, 317-324.

20. G. L. Chen, H. Qi, W. H. Xing and N. P. Xu, *J. Membr. Sci.*, 2008, 318, 38-44.

21. Y. C. Dong, B. Lin, K. Xie, S. L. Wang, H. P. Ding, D. R. Fang, X. Q. Liu and G. Y. Meng, *J. Alloys Compd.*, 2009, 477, 350-356.

22. Y. C. Dong, S. F. Chen, X. B. Zhang, J. K. Yang, X. Q. Liu and G. Y. Meng, *J. Membr. Sci.,* 2006, 281, 592-599.

23. L. Black, C. Breen, J. Yarwood, C. S. Deng, J. Phipps and G. Maitland, *J. Mater. Chem.*, 2006, 16, 1263-1272.

24. D. D. Double, A. Hellawell and S. J. Perry, *Proc. R. Soc. Lond. A*, 1978, 359, 435-451.

25. H. N. Atahan, O. N. Oktar and M. A. Tasdemir, *Constr. Build. Mater.*, 2009, 23, 1196-1200.

26. B. J. Putman and A. I. Neptune, *Constr. Build. Mater.*, 2011, 25, 3480-3485.

27. N. Neithalath, M. S. Sumanasooriya and O. Deo, *Mater. Charact.*, 2010, 61, 802-813.

28. X. H. Kuang and J. Sansalone, *Water Sci. Technol.*, 2011, 63, 2992-2998.

29. Y. H. Wang, Y. Zhang, X. Q. Liu and G. Y. Meng, *J. Sol-Gel Sci. Technol.*, 2007, 41, 267-275.

30. S. Workneh and A. Shukla, *J. Membr. Sci.*, 2008, 309, 189-195.

31. H. Qi, Y. Q. Fan, W. H. Xing and L. Winnubst, *J. Eur. Ceram. Soc.*, 2010, 30, 1317-1325.

32. Y. B. P. Kwan, D. J. Stephenson and J. R. Alcock, *J. Porous Mater.*, 2001, 8, 119-127.

33. Y. Shimada and J. F. Young, *Adv. Cem. Res.*, 2001, 13, 77-81.

34. P. Chindaprasirt, S. Thaiwitcharoen, S. Kaewpirom and U. Rattanasak, *Cem. Concr. Compos.*, 2013, 41, 24-28.

35. G. Moeschner, B. Lothenbach, F. Winnefeld, A. Ulrich, R. Figi and R. Kretzschmar, *Cem. Concr. Res.*, 2009, 39, 482-489.

36. N. Meller, C. Hall, A. C. Jupe, S. L. Colston, S. D. M. Jacques, P. Barnes and J. Phipps, *J. Mater. Chem.*, 2004, 14, 428-435.

37. G. Moeschner, B. Lothenbach, J. Rose, A. Ulrich, R. Figi and R. Kretzschmar, *Geochim. Et Cosmochim. Acta*, 2008, 72, 1-18.

38. E. Sakai, Y. Nikaido, T. Itoh and M. Daimon, *Cem. Concr. Res.*, 2004, 34, 1669-1673.

39. M. C. Almandoz, J. Marchese, P. Pradanos, L. Palacio and A. Hernandez, *J. Membr. Sci.*, 2004, 241, 95-103.

40. B. K. Nandi, R. Uppaluri and M. K. Purkait, *Appl. Clay Sci.*, 2008, 42, 102-110.

41. F. Bouzerara, S. Boulanacer, A. Harabi, B. Boudaira, S. Achour and S. Condom, *Phys. Procedia*, 2009, 2, 1449–1453.

42. I. Jedidi, S. Khemakhem, S. Saidi, A. Larbot, N. Elloumi-Ammar, A. Fourati, A. Charfi, A. Ben Salah and R. Ben Amar, *Powder Technol.*, 2011, 208, 427-432.

43. J. L. Zhang, J. G. Liu, C. Li, Y. F. Nie and Y. Y. Jin, *Cem. Concr. Res.*, 2008, 38, 675-680.

44. H. A. van der Sloot, *Cem. Concr. Res.*, 2000, 30, 1079-1096.

45. M. A. Trezza and A. N. Scian, *J. Hazard. Mater.*, 2007, 147, 188-196.

46. GB5749-2006, Ministry of Health of the People's Republic of China and Standardization Administration of the People's Republic of China, Beijing, 2006.

47. EPA 822-S-12-001, Office of Water，U.S. Environmental Protection Agency，Washington, DC, 2012.

Figure Captions

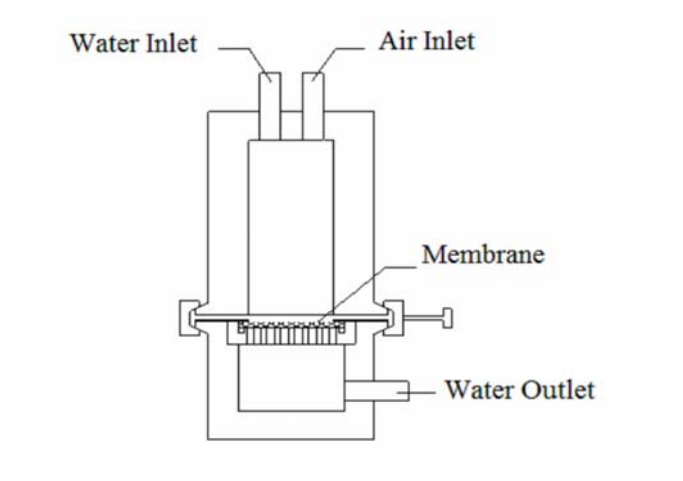

Fig. 1 Experimental setup for water filtration test.

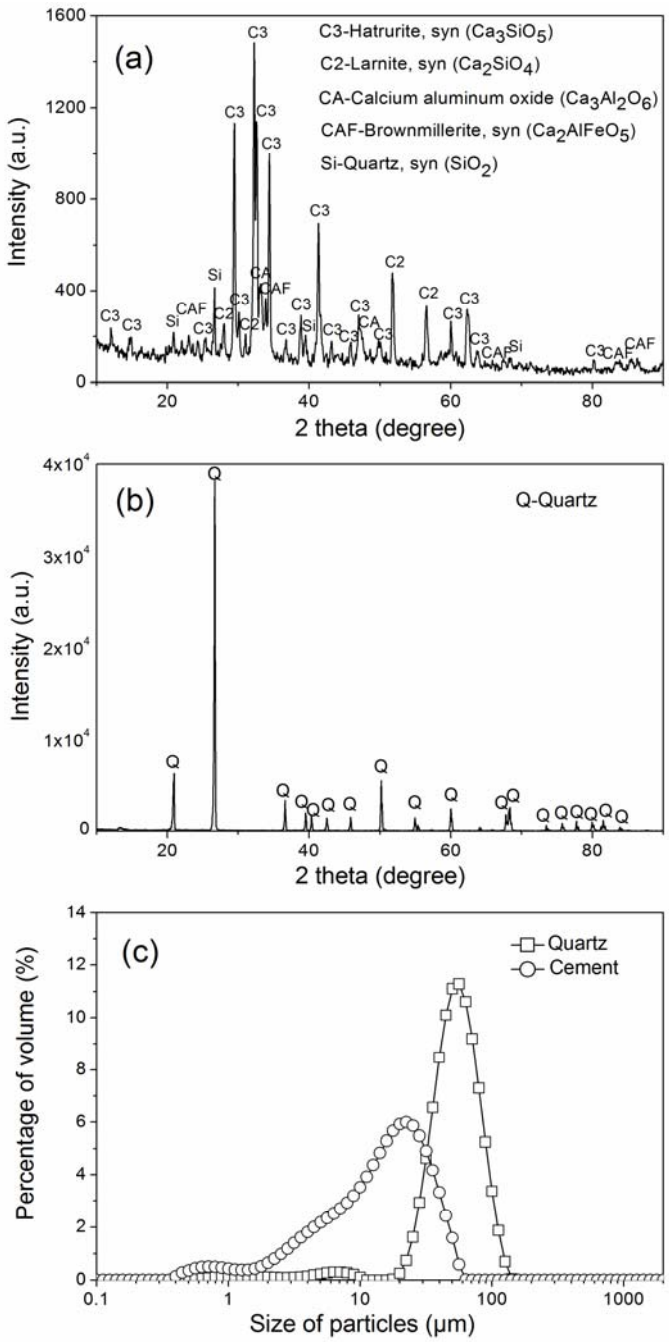

Fig. 2 Raw materials analysis. (a) XRD patterns of the cement, (b) XRD patterns of the quartz, (c) particle size distributions of the quartz and cement used.

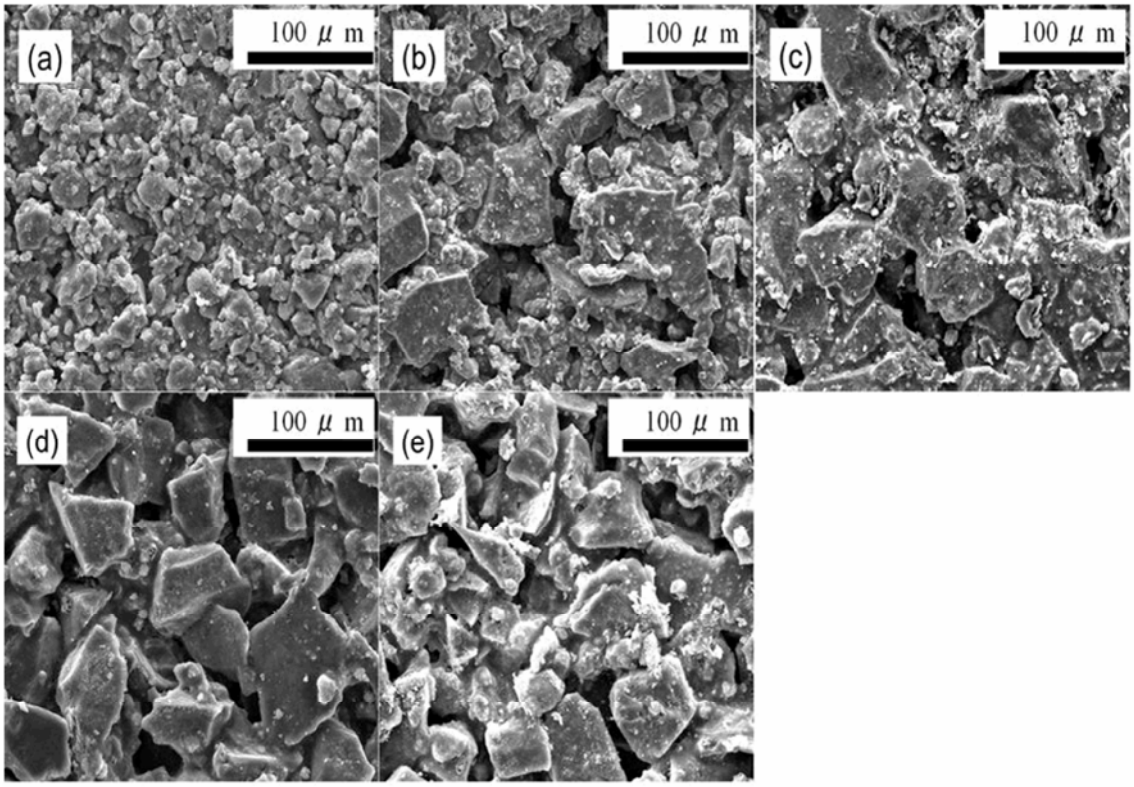

Fig. 3 SEM images (×1000) of the cementitious membrane surface. The membranes are produced at different q/c values: (a) 0.3, (b) 1.0, (c) 2.0, (d) 3.0, (e) 4.0.

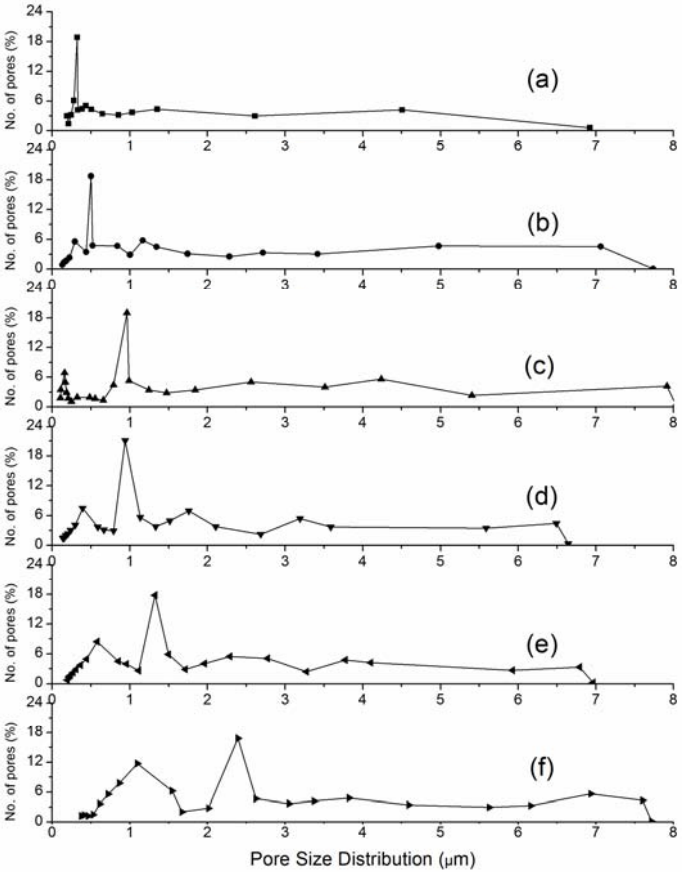

Fig. 4 Pore size distribution of the membranes fabricated at different q/c values: (a) 0.3, (b) 0.5, (c) 1.0, (d) 2.0, (e) 3.0, (f) 4.0.

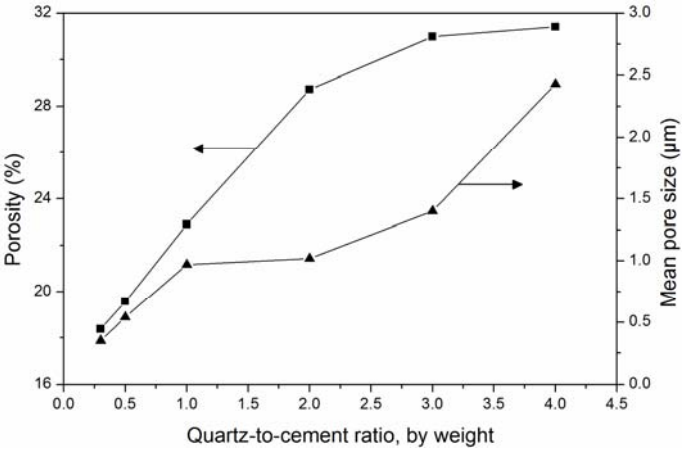

Fig. 5 Porosity and mean pore size of the membranes fabricated at different q/c values.

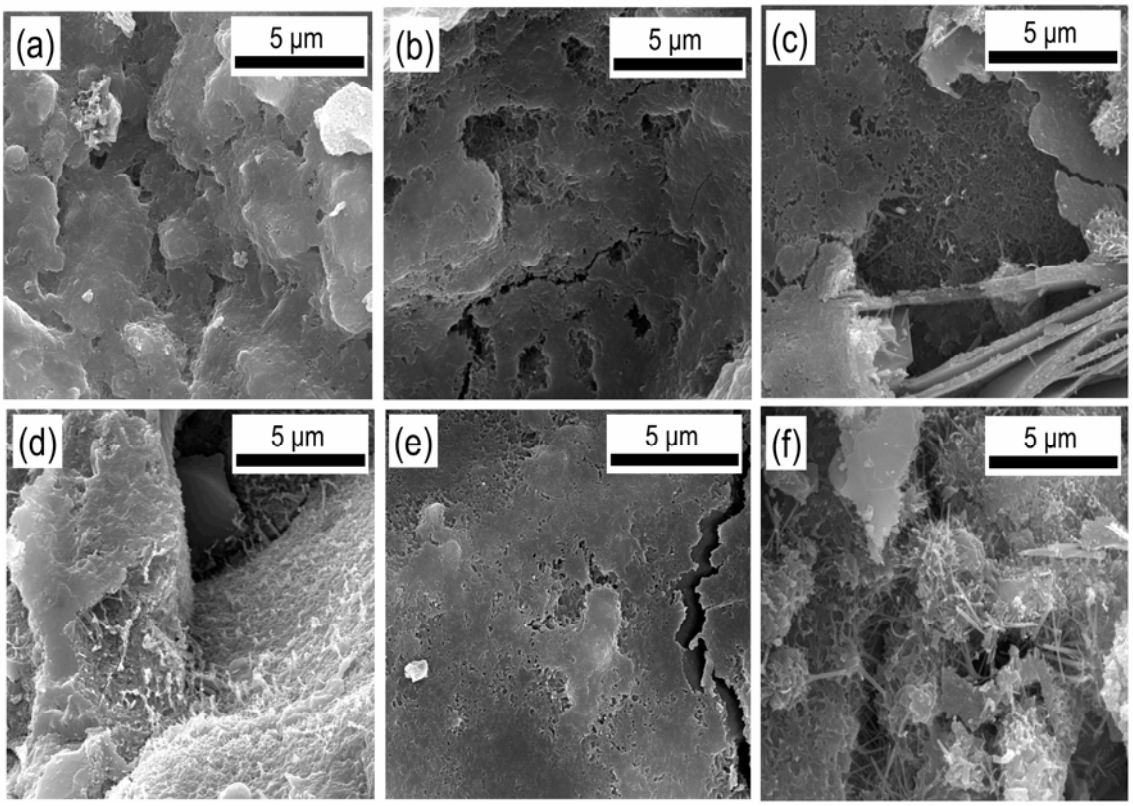

Fig. 6 SEM images (×20000) of the membrane surface and fracture, focusing on the area of cement connection. Surface images: (a) 0.3 q/c, (b) 2.0 q/c, (c) 4.0 q/c. Fracture images: (d) 0.3 q/c, (e) 2.0 q/c, (f) 4.0 q/c.

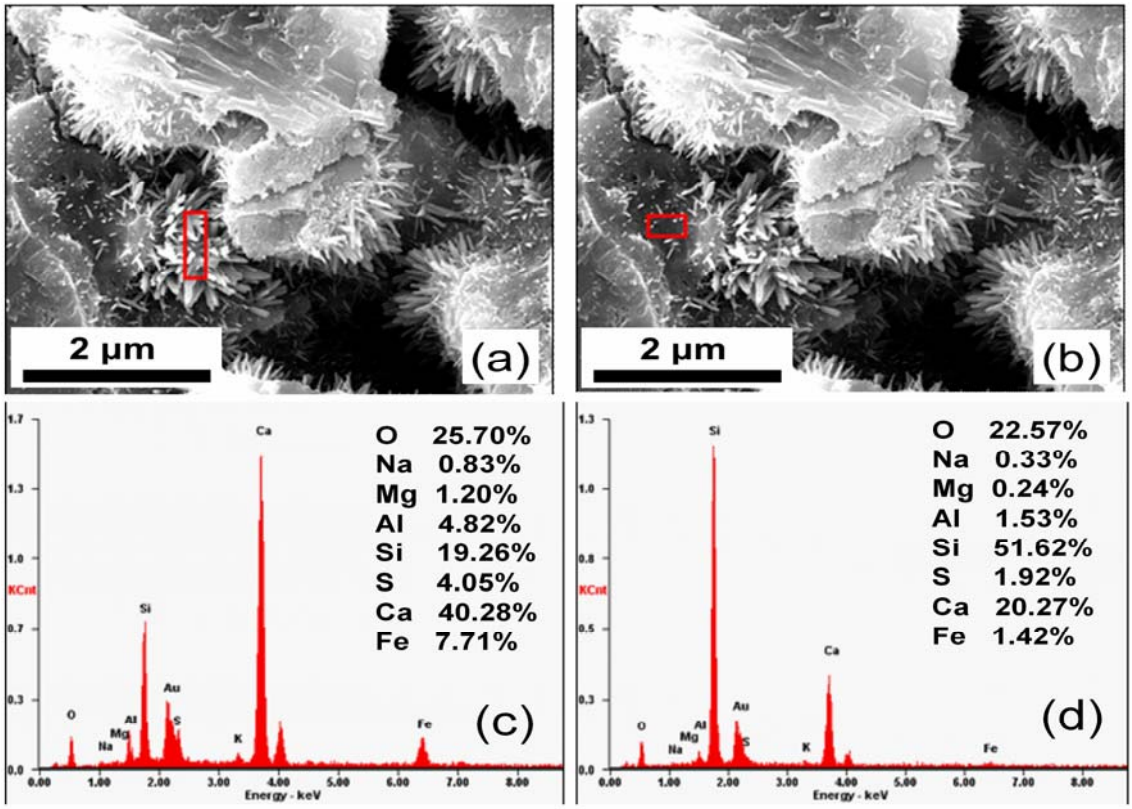

Fig. 7 EDX analysis of the membrane. (a) SEM image (×50000) of the membrane fracture, where the red box marks the needle-like structure; (b) SEM image (×50000) of the membrane fracture, where the red box marks the adjacent flat area; (c) EDX analysis results of the needle-like structure marked in (a); (d) EDX analysis results of the adjacent flat area marked in (b).

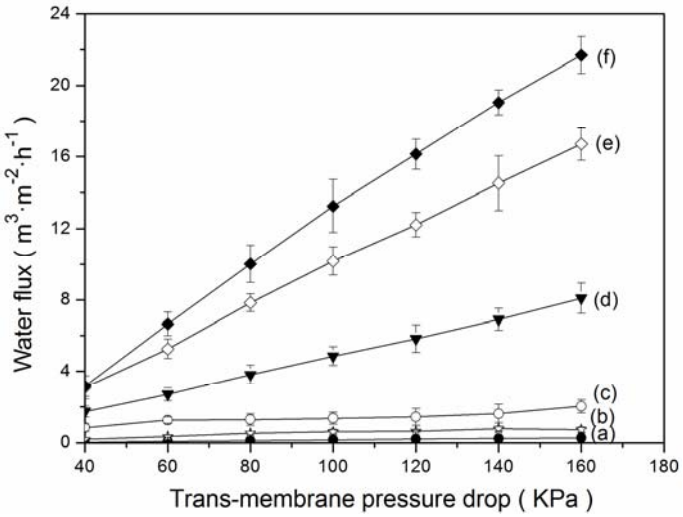

Fig. 8 Water flux of the membranes fabricated at different q/c values: (a) 0.3, (b) 0.5, (c) 1.0, (d) 2.0, (e) 3.0, (f) 4.0. The error bars indicate the standard deviation of the mean (n=3).

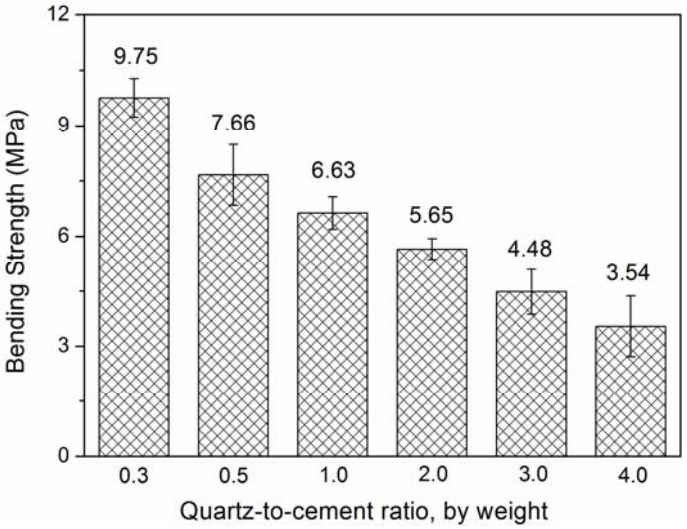

Fig. 9 Bending strength of the membranes fabricated at different q/c values. The error bars indicate the standard deviation of the mean (n=3).

Tables

Table 1 Mixture proportions of the raw materials used in the fabrication of the membrane.

	Quartz to cement ratio (q/c)	Quartz (g)	Cement (g)	Demonized water (ml)
a	0.3	10.0	30.0	7.0
b	0.5	13.3	26.7	7.0
c	1.0	20.0	20.0	7.0
d	2.0	26.7	13.3	7.0
e	3.0	30.0	10.0	7.0
f	4.0	32.0	8.0	7.0

Table 2 XRF analysis of the membrane (using a q/c of 3.0) and element dissolution analysis of the membrane effluent. Symbol "-" means no detection.

Elements	pH	Na	Mg	Al	Si	P	S	K	Ca	Cr	Mn	Fe	Cu	Zn	Sr	Pb
XRF (%)	–	0.69	0.12	0.61	19.97	0.02	1.40	0.68	7.57	0.01	0.02	0.58	0.01	0.02	0.02	0.01
Influent (mg/L)	6.45	0.05	0.03	–	0.06	0.02	0.13	0.41	0.18	–	–	–	–	–	–	–
Effluent (mg/L) (60 KPa)	6.80	0.28	0.07	0.09	0.30	0.01	1.48	0.59	6.19	–	–	–	–	–	0.01	–
Effluent (mg/L) (20 KPa)	7.21	0.73	0.07	0.13	0.70	0.01	2.60	1.16	9.18	–	–	0.01	–	–	0.02	–
GB5749-2006, China (mg/L)	6.5-8.5	200	–	0.2	–	–	–	–	–	0.05	0.1	0.3	1	1	–	0.01
EPA, USA 822-R-06-013 (mg/L)	6.5-8.5	–	–	0.05-0.2	–	–	–	–	–	0.1	0.05	0.3	1	5	–	0